

Sapropterin (BH4) aggravates autoimmune encephalomyelitis in mice

Katja Schmitz¹, Sandra Trautmann¹, Lisa Hahnefeld¹, Caroline Fischer¹, Robert Gurke¹, Yannik Schreiber¹, Robert Brunkhorst¹, Ernst Werner², Katrin Watschinger², Sabine Wicker¹, Dominique Thomas¹, Gerd Geisslinger¹, and Irmgard Tegeder¹

¹Goethe University Frankfurt

²University of Innsbruck

August 4, 2020

Abstract

Background and Purpose: Depletion of the enzyme cofactor, tetrahydrobiopterin (BH4) in T-cells was shown to prevent their proliferation upon receptor stimulation in models of allergic inflammation in mice suggesting that BH4 drives autoimmunity. Hence, the clinically available BH4 medication (sapropterin) might increase the risk of autoimmune diseases. **Experimental Approach:** The present study assessed the implications for multiple sclerosis (MS) as a model autoimmune disease in MS patients and in immunization-evoked autoimmune encephalomyelitis (EAE), a model of multiple sclerosis in mice. **Key Results:** Plasma levels of biopterin were persistently low in MS patients, and the bypass product, neopterin tended to be increased suggesting a relative deficiency of BH4. Ex vivo stimulation of human whole blood indeed led to a drop of biopterin pointing to high consumption. Hence, BH4 replenishment might either further drive the immune response or beneficially restore the BH4 balance. To answer this question, mice were treated with sapropterin in the EAE model. Sapropterin-treated mice had higher EAE disease scores associated with higher numbers of T-cells infiltrating the spinal cord, but normal T-cell subpopulations in spleen and blood, suggesting that BH4 facilitated the invasion of the central nervous system (CNS). Sapropterin-treated EAE mice had increased plasma levels of long-chain ceramides and low levels of the poly-unsaturated fatty acid, linolenic acid (FA18:3). These lipid changes are known to contribute to disruptions of the blood brain barrier in EAE mice. **Conclusion and Implications:** Sapropterin might aggravate autoimmune disease of the CNS through permissive effects at the brain barrier.

Sapropterin (BH4) aggravates autoimmune encephalomyelitis in mice

Katja Schmitz¹, Sandra Trautmann¹, Lisa Hahnefeld¹, Caroline Fischer¹, Yannik Schreiber¹, Robert Brunkhorst², Ernst R. Werner³, Katrin Watschinger³, Sabine Wicker⁴, Dominique Thomas¹, Gerd Geisslinger^{1,5,6}, Irmgard Tegeder¹

¹Institute of Clinical Pharmacology, Goethe-University, Medical Faculty, Frankfurt, Germany

²Department of Clinical Neurology, Goethe-University, Medical Faculty, Frankfurt, Germany

³Institute of Biological Chemistry, Biocenter, Medical University of Innsbruck, Austria

⁴Occupational Health Services, Goethe-University, Medical Faculty, Frankfurt, Germany

⁵Fraunhofer Institute for Molecular Biology and Applied Ecology, Branch Translational Medicine, Frankfurt, Germany

⁶Fraunhofer Cluster of Excellence for Immune mediated Diseases, Frankfurt, Germany

Correspondence

Irmgard Tegeder, MD
Goethe-University Frankfurt, Medical Faculty
Institute of Clinical Pharmacology
Theodor Stern Kai 7, 60590 Frankfurt, Germany
Ph 49 696301 7621
tegeder@em.uni-frankfurt.de

Key words

Tetrahydrobiopterin, T-cells, GTP cyclohydrolase, nitric oxide, ceramides, omega lipids

Running head

BH4 and EAE

Word count

Abstract: 247

Main body without Methods/References: 2513

Main body without References: 5170

Abstract

Background and Purpose: Depletion of the enzyme cofactor, tetrahydrobiopterin (BH4) in T-cells was shown to prevent their proliferation upon receptor stimulation in models of allergic inflammation in mice suggesting that BH4 drives autoimmunity. Hence, the clinically available BH4 medication (sapropterin) might increase the risk of autoimmune diseases.

Experimental Approach: The present study assessed the implications for multiple sclerosis (MS) as a model autoimmune disease in MS patients and in immunization-evoked autoimmune encephalomyelitis (EAE), a model of multiple sclerosis in mice.

Key Results: Plasma levels of biopterin were persistently low in MS patients, and the bypass product, neopterin tended to be increased suggesting a relative deficiency of BH4. *Ex vivo* stimulation of human whole blood indeed led to a drop of biopterin pointing to high consumption. Hence, BH4 replenishment might either further drive the immune response or beneficially restore the BH4 balance. To answer this question, mice were treated with sapropterin in the EAE model. Sapropterin-treated mice had higher EAE disease scores associated with higher numbers of T-cells infiltrating the spinal cord, but normal T-cell subpopulations in spleen and blood, suggesting that BH4 facilitated the invasion of the central nervous system (CNS). Sapropterin-treated EAE mice had increased plasma levels of long-chain ceramides and low levels of the poly-unsaturated fatty acid, linolenic acid (FA18:3). These lipid changes are known to contribute to disruptions of the blood brain barrier in EAE mice.

Conclusion and Implications: Sapropterin might aggravate autoimmune disease of the CNS through permissive effects at the brain barrier.

Abbreviations

AGMO, alkylglycerol monooxygenase; BBB, blood brain barrier; BH4, tetrahydrobiopterin; EAE, experimental autoimmune encephalomyelitis; DAHP, diaminohydroxypyrimidine; GCH1, GTP cyclohydrolase 1; MS, multiple sclerosis; NOS, nitric oxide synthase; RRMS, relapsing remitting MS; PPMS, primary progressive MS; SPMS, secondary progressive MS; PTPS, 6-pyrovoyltetrahydropterin synthase; SPR, sepiapterin reductase

Introduction

GTP cyclohydrolase, GCH1 is the rate-limiting enzyme in the de novo biosynthesis of tetrahydrobiopterin (BH4), which is an enzyme cofactor essentially required for the production of monoamine neurotransmitters and nitric oxide (Werner et al., 2011), and the metabolism of ether-lipids via alkylglycerol monooxygenase (AGMO) (Watschinger et al., 2010). The synthesis is a 3-step enzymatic cascade starting with GCH1. The downstream enzymes are PTPS (pyruvoyltetrahydropterin synthase) and SPR (sepiapterin reductase). The expression of GCH1 is increased on demand to meet requirements of BH4, which is particularly high in inflammatory conditions owing to the upregulation of inducible nitric oxide synthase in myeloid derived inflammatory cells (McNeill et al., 2015).

Recently, Cronin et al. demonstrated that GCH1 is also upregulated in activated CD4 positive and CD8+ T-cells (Cronin et al., 2018). By using T-cell-specific GCH1 depletion and overexpression, or SPR inhibition, the authors show that BH4 acts as a regulator of T-cell receptor dependent T-cell proliferation in various models of allergy, autoimmunity and immune mediated cancer surveillance (Cronin et al., 2018). GCH1 deficiency attenuated T-cell proliferation, and overexpression had opposite effects. Intriguingly, nitric oxide (NO) was apparently not involved but BH4 acted as a regulator of iron homeostasis (Cronin et al., 2018), suggested by low iron levels and low conversion of ferri Fe^{3+} to ferro Fe^{2+} . As a result, cytochrome c activity and ATG generation were reduced. Hence, the proliferation defect may originate from an energy deficit (Cronin et al., 2018).

Mostly, the authors used T-cell transfer models that skip the active immunization. T-cell transfer models do not require antigen recognition, presentation and initiation of antigen-specific T-cell proliferation. The consideration of the model is important in the light of the protective anti-oxidative and anti-inflammatory effects of BH4/sapropterin in models of cardiovascular diseases (Katusic et al., 2009; Li et al., 2011) or colitis (Zschiebsch et al., 2016), and inhibition of tumor growth upon GCH1 inhibition (Pickert et al., 2013). Sapropterin-hydrochloride (Kuvan®) is a clinically available BH4 medication approved for treatment of genetic BH4 deficiency (Howells et al., 1986; Williams et al., 1979), and was also suggested as adjunctive treatment for cardiovascular disease (Jeong et al., 2019; Rodriguez-Miguel et al., 2018), diabetes (Gangula et al., 2018), depression and schizophrenia (Clelland et al., 2020) and mycobacterial infection (McNeill et al., 2018).

The duality of results suggest that the net outcome of high or low BH4 concentrations in vivo depends on the cellular source and the complex functions in the disease-specific and site-specific (auto)-immune context. Because sapropterin is an approved drug, it is crucial to know if it boosts T-cell responses under certain conditions. In particular, autoimmune diseases of the peripheral and central nervous system such as multiple sclerosis differ from other sites because blood-to-brain and brain-to-CSF barriers normally hinder immune cells from invasion. BH4-dependent endothelial NOS is highly expressed in brain endothelial cells, and pro-oxidative metabolites that are generated via NOS in the absence of BH4, promote a disruption of the BBB (Wu et al., 2009). It is well known that MS pathophysiology has a strong oxidative contribution (Fischer et al., 2012; Licht-Mayer et al., 2015; Linker et al., 2011; Mossakowski et al., 2015). In addition to redox targets, BH4 alters bioactive lipids (Zschiebsch et al., 2016) presumably via AGMO, which are crucial for BBB integrity.

To assess the putative benefit or adversity of the currently available BH4 drug (sapropterin, Kuvan®), we used the experimental autoimmune encephalomyelitis (EAE) model, in which the MS like disease is evoked by active immunization against proteins of myelin sheaths. We analyzed the disease course, immune cell proliferation, and invasion and alterations of lipid signaling molecules. The mechanistic focus on bioactive lipids was motivated by the functions of AGMO in inflammation and resolution (Watschinger et al., 2015) and iron dependency of fatty acid metabolism.

Methods

Patients with multiple sclerosis and healthy controls

Human samples and biographic data were available from an observational cross-sectional investigation including 102 multiple sclerosis (MS) patients (31 men, 71 women) as described in (Schmitz et al., 2017; Schmitz et al., 2019). They were consecutively recruited from outpatients and inpatients of the Department of Neurology of the Goethe University Hospital Frankfurt, Germany. Data and blood collection was part of the local bio-banking project (Neurological Department of the Goethe University, Frankfurt). The diagnosis of MS was based on ICD10 criteria. Additional 14 patients with serious disease courses were recruited and observed up to 3.5 years for time course analyses. The patients participated in clinical efficacy studies of fingolimod or natalizumab (NTZ).

To cover the whole period, control samples were analyzed from four consecutive cohorts of healthy subjects (HC). The first encompassed 117 men and 233 women with a mean age of 28 ± 8 years (range 18-57 years). The second were 118 men and 183 women, aged 25 ± 6 years (range 18 - 57 years), the third were 108 m, 217 f with a mean age of 35 ± 12.8 years (range 18-68 years), and the last cohort comprised each 25 men and women above 50 years of age (mean \pm SD: 62.9 ± 8.4 years, range 50-79). HC cohorts 1 to 3 were recruited through the Occupational Health Service at the University Hospital of Frankfurt, Germany. HC cohort-4 was recruited from family, friends and colleagues.

For the whole blood assay, venous blood of healthy donors was sampled in K⁺-EDTA tubes (Tegeder et al., 2008), each split into two samples, one stimulated with 10 μ g/ml LPS, the other unstimulated and kept in a 37°C water bath for the indicated times, and biopterin was analyzed in plasma.

The studies were approved by the Ethics Committee of the Medical Faculty of the Goethe University and adhered to the Declaration of Helsinki. Informed written consent was obtained from each participating subject. Venous blood samples were collected to K⁺ EDTA tubes or in serum tubes and centrifuged at 3000 rpm for 10 min. Plasma and serum were frozen at -80°C up to analysis.

Animals and drug treatments

Female 10-12 weeks old SJL/J mice (Charles River, Germany) were used for study of relapsing-remitting EAE, and C57Bl6/J mice (Charles River, Germany) were used for the study of primary progressive EAE. Mice were housed at 2-4 mice per cage at constant room temperature (21 ± 1 °C) under a regular light/dark schedule with light from 7:00 A.M. to 7:00 P.M. Food and water were available *ad libitum* .

For the treatment of SJL/J-EAE mice, DAHP (Sigma #D19206; 4 mg/day, 200 mg/kg/d) or BH4 (Sigma #T4425; 2 mg/day, 100 mg/kg/d) were dissolved in the drinking water with 2% DMSO. Control animals received the respective vehicle. In C57Bl6/J-EAE mice, BH4 was administered perorally once daily in cornflakes soaked with 10% sucrose/5% ethanol in water. Treatments started at the day of immunization. Control animals received the respective vehicle.

AGMO LacZ reporter mice were used to assess the localization of AGMO in the brain and were created according to EUCOMM gene targeting strategy (Coleman et al., 2015).

The experiments were approved by the local Ethics Committee for Animal Research (Darmstadt, Germany) and adhered to the European guidelines and to those of GV-SOLAS for animal welfare in science and agreed with the ARRIVE guidelines.

EAE model

SJL/J female mice were immunized using the Hooke Kit 2110PLP139-151/CFA emulsion PTX (EK-2120, Hooke Labs, St Lawrence, MA), which contains 200 μ g of peptide 139-151 of myelin proteolipid protein (PLP)

emulsified in 200 μ l Complete Freund's Adjuvant (CFA). The emulsion was injected subcutaneously (s.c.) at two sites followed by two intraperitoneal (i.p.) injections of 200 ng pertussis toxin (PTX) in phosphate buffered saline (PBS), the first 1-2 h after and the second 24 h after PLP₁₃₉₋₁₅₁.

C57Bl6/J female mice were immunized using Hooke KitTMMOG₃₅₋₅₅/CFA emulsion PTX (EK-2110), which contains 200 μ g of a peptide 35-55 (amino acids) of myelin oligodendrocyte glycoprotein (MOG) in 200 μ l CFA (Hooke Labs, US). Injections of the emulsion and PTX were done as described above.

EAE scores were assessed daily to evaluate the severity and extent of motor function deficits. Score 0, normal motor functions; score 0.5, distal paralysis of the tail; score 1, complete tail paralysis; score 1.5, mild paresis of one or both hind legs; score 2, severe paresis of one or two hind legs; score 2.5, complete paralysis of one hind leg; score 3, complete paralysis of both hind legs; score 3.5, complete paralysis of hind legs and paresis of one front leg.

Blood and tissue samples were obtained at the end of the clinical observation time, 19-22 days after immunization. Blood was collected in K⁺ EDTA microtubes (EDTA K⁺ Microvette Sarstedt), centrifuged at 3000 rpm for 10 min and stored in standard Eppendorf caps at -80°C until analysis. Tissue samples were snap frozen on dry ice and stored at -80°C until lipid analysis or they were freshly prepared for FACS.

FACS analysis of surface marker proteins

Single cell suspensions were prepared from the spleen, and the lumbar spinal cord. Tissues were rapidly dissected, treated with lysis buffer (DMEM/acutase (PAA) 1:1, collagenase (3 mg/ml, Sigma), DNase I (1U/ml, Promega)) for 30 min at 37°C, followed by mechanical disruption, which was done by forcing the tissue through a nylon mesh with 70 μ m pore size (Cell Strainer, BD). Cell suspensions were mixed with 1 ml erythrocyte lysis buffer for 10 min at room temperature and CD16/32 blocking antibody (Fc γ RII/III receptor blocker, BD) for 15 min on ice. For staining of cell surface antigens, cells were incubated for 20 min at room temperature in staining buffer with the respective fluorochrome labeled antibodies (Suppl. Table 1) and were then counted with a flow cytometer (BD FACS Canto II). FACS scans were analyzed with FlowJo 10.6. For all FACS assays, antibody concentrations followed the recommendations of the manufacturers and the controls were FITC, PE, or APC-conjugated rat IgG.

Immunofluorescence analyses and LacZ histology

A subset of mice were used for histology. Mice were terminally anaesthetized with isoflurane and cardially perfused with cold 0.9% saline, followed by 4% paraformaldehyde (PFA) in 1x PBS for fixation. The lumbar spinal cord was excised, post-fixed in 4% PFA for 2 h, cryoprotected overnight in 20% sucrose at 4 °C, embedded in tissue molds in cryomedium and cut on a cryotome (12 μ m). Slides were air-dried and stored at -80°C. After thawing, slides were immersed and permeabilized in 1x PBS with 0.1% Triton-X-100 (PBST), then blocked with 3% BSA in PBST, subsequently incubated overnight with the first primary antibody in 1% BSA in PBST at 4°C, washed and incubated with the secondary fluorochrome-labelled antibody (Alexa488 or Cy3) for 2 h at room temperature. The procedure was repeated for further antibody pairs, followed by 10 min incubation with 1 μ g/ml DAPI and embedding in Fluoromount (eBioscience).

For beta galactosidase (LacZ) visualization in tissue sections of AGMO-LacZ reporter mice, cryosections were postfixed for 5 min in 2% PFA, washed in 1x PBS with 2 mM MgCl₂ and 3 times in washing buffer containing detergent (1x PBS/2 mM MgCl₂ with 0.1 % sodium deoxycholate, 0.02% Nonidet P40, pH 7.5) for 5 min at room temperature. Slides were then incubated at 37°C with the staining solution consisting in 0.5 mg/ml nitrotetrazolium blue chloride (NTB), 5 μ g/ml phenazine methosulfate (PMS) in detergent washing solution. The incubation time was adjusted to the tissue. The reaction was stopped by washing the slides 3x in 1x PBS for 5-10 min. Slides were counter-stained with eosin, dehydrated in increasing ethanol concentrations and xylene before embedding in Pertex mounting medium.

Tiled images were captured (10x objective lens) on an inverted fluorescence microscope (BZ-9000, KEYENCE, Germany), and were stitched using the Keyence's software to cover the complete spinal cord. Filter and acquisition parameters were set to assure comparability. Subsequently, higher magnification images (20x objective lens) of the grey-to-white matter border were obtained of various regions. CD3+ T-cells were quantified using the particle counter plugin of FIJI ImageJ after background subtraction and threshold setting according to the IJ IsoData algorithm implemented in FIJI. Zoom-in images (5x) were created from regions of interest. The area covered by immunoreactive cells relative to the total area (which was identical in all images) was used to assess treatment effects. Three or more non-overlapping images of three mice were analyzed per group.

Culture of splenocytes

Spleen tissue was rapidly dissected, treated with lysis buffer (DMEM/acutase (PAA) 1:1, collagenase (3 mg/ml, Sigma), DNase I (1U/ml, Promega)) for 30 min at 37°C, followed by mechanical disruption, which was done by forcing the tissue through a nylon mesh with 70 µm pore size (Cell Strainer, BD). Cell suspensions were washed, resuspended in PBS and the cell number was counted with a Neubauer chamber. 5×10^5 cells were plated, cultured in RPMI1640-GlutaMax medium (GibcoTM, Life technologies) and restimulated with 25 ng/ml IFN γ for 24 h.

Griess assay of nitric oxide

The concentration of nitrite/nitrate was determined with the Saville-Griess assay adapted for microtitre plates. A standard curve was prepared with serial dilutions (0–50 µM) of a freshly prepared sodium nitrite (NaNO₂) stock solution (100 mM). Cells were homogenized in 1x PBS and, after centrifugation, 200 µl of the supernatant were added to a well of a 96-well plate. 50 µl of sulfanilamide solution (4mg/ml in 1N HCl) were added to standards and samples. After 2 min incubation, 50 µl of N-(naphthyl)-ethylenediamine dihydrochloride solution (6 mg/ml in H₂O) were added, followed by incubation for 5 min at room temperature and measuring absorbance at 540 nm with a Specta Fluor Plus[®] instrument and XFluor[®] software (Tecan, Crailsheim).

Analysis of lipid signaling molecules

Bioactive lipids including sphingolipids and ceramides, lysophosphatidic acids and endocannabinoids were analyzed by liquid chromatography-electrospray ionization-tandem mass spectrometry (LC-ESI-MS/MS) as described in detail in the supplementary material of (Brunkhorst-Kanaan et al., 2019). All analytical methods were optimized based on previous methods (Brunkhorst-Kanaan et al., 2019; Schmitz et al., 2017; Zschiebsch et al., 2016).

In brief, the analytes were extracted using liquid-liquid-extraction. Sample volumes were 10 µl for sphingolipids, 50 µl each for LPA and 100 µl for endocannabinoids. The quantification of all analytes was performed using a hybrid triple quadrupole-ion trap mass spectrometer QTRAP 5500 or 6500+ (Sciex, Darmstadt, Germany) equipped with a Turbo-V-source operating in positive ESI mode for sphingolipids and endocannabinoids and in negative ESI mode for LPA.

Sphingolipids were separated using an Agilent 1200 HPLC system equipped with a Zorbax C18 Eclipse Plus UHPLC column (50 × 2.1 mm, 1.8 µm, Agilent technologies, Waldbronn, Germany) and the analysis of LPA was done on the same HPLC system using a Luna C18 column (50 × 2 mm, 5 µm, Phenomenex, Aschaffenburg, Germany). Analysis of the endocannabinoids was done using an Agilent 1290 Infinity I UHPLC system equipped with an Acquity UPLC BEH C18 UPLC column (100 × 2.1 mm, 1.7 µm, Waters, Eschborn, Germany).

Quality control samples of three different concentration levels (low, middle, high) were run as initial and final samples of each run. For all analytes, the concentrations of the calibration standards, quality controls and

samples were evaluated by Analyst software 1.6.3 and MultiQuant software 3.0.2 (Sciex) using the internal standard method (isotope-dilution mass spectrometry) as described in (Gurke et al., 2019). Variations in accuracy were less than 15% for at least 67% of all QC samples. For the lower limit of quantification, a variation of 20% was accepted.

Untargeted lipidomic analyses

Twenty microliter plasma or 40 μ l lymph nodes homogenates (homogenated in 0.025 μ g/ml water:ethanol 1:3 (v/v)) were extracted using methyl-tert-butyl-ether (Matyash et al., 2008). The organic phase was split into two aliquots, one for analysis in negative ion mode and the other in positive ion mode. After drying under a nitrogen stream at 45°C, the aliquots were reconstituted in 120 μ l methanol or stored at -40°C until analysis. LC-MS analysis was performed on a Nexera X2 system (Shimadzu Corporation, Kyoto, Japan) coupled to a TripleTOF 6600 (Sciex). The chromatographic separation was done on a Zorbax RRHD Eclipse Plus C8 1.8 μ m 50x2.1 mm ID column (Agilent, Waldbronn, Germany) with a SecurityGuard Ultra C8 pre-column (Phenomenex, Aschaffenburg, Germany), using a binary gradient with 40°C column temperature and a flow rate of 0.3 ml/min. For the positive mode, the mobile phase A consisted of 10 mM ammonium formate and 0.1% formic acid in water and mobile phase B of 0.1% formic acid in acetonitrile: isopropanol 2:3 (v/v). For measurement in negative mode 1 mM ammonium formate and 0.1% formic acid in water was used as for mobile phase A. The MS analysis encompasses a TOF MS Scan from 100-1000 m/z with six data dependent acquisitions per cycle and a mass range of 50 – 1000 m/z. The identification of the lipid species was based on the exact mass (+/- 5 ppm), the isotope ratio and the comparison of the MS/MS spectra with the reference spectra according to LIPID MAPS (<http://www.lipidmaps.org>), METLIN (<http://metlin.scripps.edu>) or the Human Metabolome Database (HMDB, version 4.0).

To reduce the impact of small variations in instrument sensitivity during the measurements all samples were randomized prior to analysis. Quality control samples were injected at the start and at the end of a run and after every 10th sample to verify system stability. Data evaluation was done with Analyst TF 1.7 and MultiQuant software 3.0, and peak areas were normalized to the quality control samples using median peak ratios by MarkerView software 1.2 (all Sciex).

Microarray data analysis

Microarray data of GEO dataset GSE60847 (own previous data) were reanalyzed and searched for genes involved in lipid metabolisms, regulation or function. Normalized data were analyzed with ArrayStar, which uses general linear models to assess differential expression. Data were log₂ transformed, scored according to "fold-regulation", P-value and abundance and top scored genes were then clustered using Euclidean distance metrics. Valid genes are displayed as Volcano plots, showing the log₂ difference i.e. fold change (positive for upregulated genes and negative for downregulated genes) versus the -log₁₀ of the t-test P value. The P value was set at 0.05 and adjusted according to Benjamini Hochberg. Genes were text-filtered based on gene descriptions and GO ontology terms to find lipid regulating and metabolizing genes and genes involved in BH4 pathways (synthesis, recycling and coenzyme functions).

Statistics

Group data are presented as mean \pm SD or median \pm IQR for non-parametric data as specified in the respective figure legends. Data were analyzed with SPSS 24 and Graphpad Prism 8.0 and Origin Pro 2020. Data were mostly normally distributed, or log-normally distributed. For testing the null-hypothesis that groups were identical, two groups were compared with 2-sided, unpaired Student's t-tests. The Mann Whitney U test (2 groups) or Kruskal Wallis (> 2 groups) were used as non-parametric alternatives in case of violations of t-test requirements. Time course data or multifactorial data were submitted to 2-way analysis of variance (ANOVA) using e.g. the factors 'time' and 'genotype'. In case of significant differences, groups were mutually compared at individual time points using post hoc t-tests according to Dunnett, i.e. versus the control group,

or according to Šidák. For time courses of non-parametric scores, the Friedmann test was used. Asterisks in figures show multiplicity-adjusted P-values.

Multivariate analyses of multiple lipid classes were used to reduce the dimensionality. Because raw lipid concentrations of different classes differ by several orders of magnitude, lipids were normalized and are expressed as percentage of the 90%-quantile. Canonical discriminant analysis (CanDisc) was employed to separate treatment groups and to assess the predictability of group membership. Partial least square (PLS) analysis was used if analytes exceeded the number of samples per group. Score plots and 95% confidence ellipses were created in OriginPro. Untargeted lipidomic data (normalized peak areas) were log2 transformed. Volcano plots were used to show the log2 difference (fold difference) versus the $-\log_{10}$ of the t-test P-value. Lipids of interest were further analyzed using 2-way ANOVAs for "lipid X treatment", and subsequent t-test for "treatment".

Results

Persistently low biopterin and high neopterin plasma levels in multiple sclerosis patients

Neopterin is used as activity and prognostic marker in inflammatory diseases, cancer, some infections and rheumatoid arthritis (Altindag et al., 1998; Husain et al., 2013; Prat et al., 2008; Sucher et al., 2010). Neopterin is produced in excess if the activity and expression of GCH1 exceeds the capacity of the two downstream enzymes (PTPS and SPR) to convert the GCH1 product, neopterin-3-phosphate (neopterin-3P) into BH4. Excess neopterin in serum or plasma mainly originates from activated immune cells. Overall, MS patients had increased neopterin levels (Fig. 1A), but there was no obvious association with the clinical disease activity (Fig. 1B, 1C). In parallel, biopterin levels were persistently reduced (Fig. 1A-C), but there was no inverse direct association of high neopterin with low biopterin, except in few patients (Fig. 1C). High neopterin but low biopterin suggested excessive consumption of BH4 presumably in activated immune cells. In support, biopterin levels dropped over time in human whole blood assays stimulated with LPS (Fig. 1D), and microarrays of the spinal cord of EAE mice showed increased GCH1 but reduced RNA levels of the recycling enzyme, quinoid dihydropteridine reductase (QDPR) (Suppl. Fig. 1).

The pterin data of MS patients suggested two alternative therapeutic interpretations assuming that the biopterin/neopterin balance regulates immune functions, which is strongly suggested by previous publications (Cronin et al., 2018; Huber et al., 1984; Schoedon et al., 1986). Either the supplementation with BH4 may beneficially restore normal antioxidative capacity of BH4 and iron homeostasis, or supplementation may further stimulate immune cell proliferation and activity and increase the autoimmune attack. To answer this question we used two models of autoimmune encephalomyelitis in mice (EAE), with relapsing remitting (RR-EAE; SJL mice) or primary progressive (PP-EAE; C57BL6 mice) course of the disease.

Sapropterin (BH4) treatment aggravates EAE in mice

Mice were treated with sapropterin (BH4) or DAHP (GCH1-inhibitor) or vehicle perorally starting at the day of immunization. Sapropterin treated mice reached higher maximum scores in SJL RR-EAE mice (Fig. 2A) and in C57BL6 PP-EAE mice (Fig. 2B) and increased the frequency of mice with high scores. DAHP oppositely reduced scores during the first relapse (Fig. 2A). Both drugs had no effects on body weights. The C57BL6 experiment was done with vehicle and sapropterin only.

BH4 treatment mildly increases infiltration of lymphocytes in the spinal cord in EAE mice

The observed increase of EAE scores in sapropterin-treated mice was associated with a higher number of T-cells infiltrating the lumbar spinal cord white matter, which was revealed by FACS analyses (Fig. 3A, B) and immunofluorescence analyses (Fig. 4). Both CD4+ and CD8+ T-cells were increased. FACS results for individual myeloid cell populations were not significant, but immunofluorescence studies suggested more hotspots of cellular invasion, in particular with staining of CD11b (activity marker) and F4/80 (Fig. 4). Overall proliferation of T-cells and myeloid cells in the spleen was however not affected by sapropterin or DAHP treatment as compared to vehicle treated EAE mice (Suppl. Fig. 2), suggesting that oral BH4 medication did not reinforce T-cell proliferation but was permissive for CNS infiltration. We therefore asked how BH4 medication could affect BBB integrity.

We have two major hypotheses (i) high levels of circulating BH4 activate endothelial NOS (NOS3) at the BBB, facilitating BBB breakdown (Wu et al., 2009) or (ii) BH4 leads to changes of lipid homeostasis thereby affecting barrier functions. The second hypothesis is based on its coenzyme function for AGMO (Watschinger et al., 2015) and our previous studies in colitis mice where BH4/DAHP altered LPAs and ceramides (Zschiebsch et al., 2016), both clinically relevant for MS (Kurz et al., 2018; Schiffmann et al., 2012; Schmitz et al., 2017). Because NO likely has dual effects in EAE (Giovannoni et al., 1998; Wu et al., 2009) we opted for the putative lipid-paths. It is of note that eNOS is localized at the BBB in endothelial cells (Thiel et al., 2001) whereas AGMO is strongly expressed in choroidal cells at the brain-to-CSF barrier (Suppl. Fig. 4).

Sapropterin (BH4) treatment leads to increased long-chain ceramides in EAE mice

We reanalyzed our previous microarray data of EAE versus naïve mice (Schmitz et al., 2014) (GEO dataset GSE60847) for search of lipid metabolizing genes. The RNA studies of the lumbar spinal cord revealed previously not recognized deficits in EAE of fatty acid desaturases (FADS and stearoyl CoA desaturases SCD1, SCD2) and fatty acid elongases (ELOVL) (Fig. 5A), but increased glucocerebrosidase (GBA) that degrades glucosylceramides (Fig. 5A). GCH1 was increased as expected as well NOS2 and NOS3 (Suppl. Fig. 1). The loss of desaturases, in particular FADS1, which is involved in FA18:2 and FA18:3 generation (linoleic and linolenic acid), is remarkable in light of the protective preserving effects of these omega-lipids in EAE and/or human MS (Bittner et al., 2013; Bjornevik et al., 2019).

A lipidomic screen of plasma and lymph nodes of EAE mice treated with sapropterin or vehicle revealed lipid alterations in plasma but not in the lymph nodes in sapropterin versus vehicle treated EAE mice (Suppl. Fig. 3). In plasma, polyunsaturated fatty acids, in particular linolenic acid (FA18:3), were reduced in sapropterin treated mice (Fig. 5B, 5C). It is of note, that feeding of mice with linolenic acid preserves the BBB in EAE mice because it restores gating properties of TASK1 two-pore potassium channels (Bittner et al., 2009).

Targeted LC-MS/MS lipidomic analyses were used to assess signaling lipids in more detail (Fig. 5D-F; Suppl. Fig. 3C). Using lipid species of five classes (28 different species) as input, canonical discriminant analysis clearly separated groups and allowed a >95% correct prediction of group membership based on the first two CanDisc scores (Fig. 5D). The clear separation was based mainly on ceramides of different chain lengths. Ceramides were increased in sapropterin treated EAE mice and oppositely regulated in DAHP-treated mice as compared to vehicle (Fig. 5E). Sapropterin also increased the pro-inflammatory endocannabinoid, 2-AG (Fig. 5E right), whereas DAHP reduced ethanolamide endocannabinoids (AEA and OEA). Polar plots give an overview of multiple bioactive lipid species (Fig. 5F) and reveal an increase of ceramides and unsaturated LPAs in sapropterin-treated mice, whereas lipids were mostly normal in DAHP treated mice. Scatter plots of the concentrations of individual mice are shown in Suppl. Fig. 3C. Ceramide homeostasis is crucial for the maintenance of plasma membrane integrity (Silva et al., 2007) and increased levels suggest leaky membranes and dysfunctions of lysosomal breakdown (Rao et al., 2007). Because the alterations were evident in plasma,

it is a systemic effect reaching the BBB and likely affecting membrane attachment and invasion of immune cells.

Discussion

We show in the present study that patients with MS at different stages have reduced serum biopterin levels and temporarily increased neopterin concentrations suggesting high turnover and consumption, which is supported by a drop of biopterin *ex vivo* upon immune stimulation of human whole blood. Previous studies show that BH4 assists in NRF2 (nuclear factor erythroid 2-related factor 2) activation (Gangula et al., 2018; McNeill et al., 2015), which is a key mechanism of recently used MS drugs, fumaric acid esters (Linker et al., 2011). Hence, sapropterin supplementation might foster NRF2 with beneficial clinical outcome. However, we found that oral sapropterin (BH4, Kuvan®) treatment in mice mildly aggravated immunization-evoked EAE and increased the numbers of infiltrating T-cells in the spinal cord, without effect on overall numbers in blood and spleen. The EAE results suggest that sapropterin facilitated the invasion of T-cells into the CNS, via effects on the BBB rather than direct effects on T-cells. Sapropterin medication is safe and well tolerated in phenylketonuria patients (Feillet et al., 2008; Howells et al., 1986) and did not increase T-cell proliferation, but possibly needs to be used with caution in patients with autoimmunity. Although mechanistically different, this conclusion is supported by a previous study showing that BH4 deficient T-cells have a proliferation defect (Cronin et al., 2018), owing to a defect of mitochondrial iron transport and cytochrome C functions (Cronin et al., 2018).

Mechanistically we focused on systemic alterations of lipid signaling molecules and metabolic lipids rather than iron-mediated direct effects on T-cells because we have previously observed lipid alterations in a colitis model in dependence of BH4 (Zschiebsch et al., 2016) and AGMO is abundant in epithelial barriers. Epidemiology studies suggest beneficial effects of PUFAs in MS (Bjørnevik et al., 2017), in particular linolenic acid, which was neuroprotective in EAE mice (Bittner et al., 2013), and is generated via cytochrome B5 dependent stearyl CoA desaturases and other fatty acid desaturases.

Indeed, gene expression analysis of spinal cord from EAE versus naïve mice revealed reduced levels of fatty acid desaturases and stearyl-CoA desaturase (FADS1, SCD1 and SCD2) in EAE mice. SCD mediated desaturation is carried out with help of cytochrome B5 and is dependent on iron cycling. Like AGMO, it is a transmembrane ER enzyme that generates linolenic acid (FA18:3) from linoleic acid (FA18:2) (among others), hence linking iron, BH4 and lipid metabolism. Incorporation of PUFAs into biological barriers increases membrane fluidity and facilitates the insertion of receptors (Das et al., 2003).

Mice treated with sapropterin had lower plasma levels of linolenic acid, which plays an important role in BBB maintenance in the EAE model (Bittner et al., 2009) and has been suggested as supportive diet in MS (Bjørnevik et al., 2019). In addition, sapropterin therapy in EAE was associated with an increase of plasma ceramides, which have been previously associated with the severity of EAE (Eberle et al., 2014; Schiffmann et al., 2012) suggesting that these changes are a biological correlate of the sapropterin-caused aggravation of the disease. They are not necessarily direct effects of BH4 on ceramide metabolism. Overall, the lipid alterations and clear discrimination of treatment groups based on lipids appear to be too strong to be mechanistically not linked with sapropterin. Lipid alterations may arise from changes of BH4-cofactor availability for the ER-localized lipid-metabolizing enzyme, AGMO. We observed high expression of AGMO in a LacZ reporter mouse at the brain-to-CSF barrier in the ependymal epithelium (Suppl. Fig 4), whereas endothelial NOS is highly expressed in brain endothelial cells and important for BBB functions (Wu et al., 2009). Hence, BH4 may act at two crucial barrier sites in the CNS and result in a permissive effect on immune cell invasion of the CNS. It is of note that oral sapropterin treatment in mice did not have such permissive effects on T-cell infiltration of the lamina propria in dextran sulfate sodium (DSS) evoked colitis model (Zschiebsch et al., 2016). The intestinal epithelial barrier and BBB differ in microenvironments, mesodermal versus endodermal origin and the molecular composition of the tight junctions (Daneman et al., 2009) and likely lipid composition of the membranes, which however has not yet been directly compared. Omega-3 lipids

are protective at both sites (Bjornevik et al., 2019; Zhao et al., 2015) and high ceramides are detrimental at both sites (Oertel et al., 2017; Schiffmann et al., 2012). We hypothesize that the differences rely in the model per se. EAE is autoimmune driven whereas DSS disrupts the mucous layer and gives microbiota access to the intestinal wall. Oral sapropterin might also directly affect the gut microbiome. It is important that sapropterin treatment did not increase T-cell proliferation. Hence, it was not a general "immune boost". We infer that oral sapropterin is safe as supplementation, albeit possibly with caution with autoimmune-directed CNS disease.

References

- Altindag ZZ, Sahin G, Inanici F, & Hascelik Z (1998). Urinary neopterin excretion and dihydropteridine reductase activity in rheumatoid arthritis. *Rheumatol Int* 18: 107-111.
- Bittner S, Meuth SG, Gobel K, Melzer N, Herrmann AM, Simon OJ, *et al.* (2009). TASK1 modulates inflammation and neurodegeneration in autoimmune inflammation of the central nervous system. *Brain* 132: 2501-2516.
- Bittner S, Ruck T, Schuhmann MK, Herrmann AM, Moha ou Maati H, Bobak N, *et al.* (2013). Endothelial TWIK-related potassium channel-1 (TREK1) regulates immune-cell trafficking into the CNS. *Nat Med* 19: 1161-1165.
- Bjornevik K, Chitnis T, Ascherio A, & Munger KL (2017). Polyunsaturated fatty acids and the risk of multiple sclerosis. *Mult Scler* 23:1830-1838.
- Bjornevik K, Myhr KM, Beiske A, Bjerve KS, Holmøy T, Hovdal H, *et al.* (2019). α -Linolenic acid is associated with MRI activity in a prospective cohort of multiple sclerosis patients. *Mult Scler* 25: 987-993.
- Brunkhorst-Kanaan N, Klatt-Schreiner K, Hackel J, Schroter K, Trautmann S, Hahnefeld L, *et al.* (2019). Targeted lipidomics reveal derangement of ceramides in major depression and bipolar disorder. *Metabolism* 95: 65-76.
- Clelland CL, Kantrowitz JT, Choo T, Clelland JD, & Lieberman JA (2020). Adjunctive sapropterin dihydrochloride treatment in schizophrenia: A positive proof-of-concept, rater-blind, randomized, multivitamin-controlled study. *Schizophr Res* 218: 321-323.
- Coleman JL, Brennan K, Ngo T, Balaji P, Graham RM, & Smith NJ (2015). Rapid Knockout and Reporter Mouse Line Generation and Breeding Colony Establishment Using EUCOMM Conditional-Ready Embryonic Stem Cells: A Case Study. *Front Endocrinol (Lausanne)* 6: 105.
- Cronin SJF, Seehus C, Weidinger A, Talbot S, Reissig S, Seifert M, *et al.* (2018). The metabolite BH4 controls T cell proliferation in autoimmunity and cancer. *Nature* 563: 564-568.
- Daneman R, & Rescigno M (2009). The gut immune barrier and the blood-brain barrier: are they so different? *Immunity* 31:722-735.
- Das G, Augustine MM, Das J, Bottomly K, Ray P, & Ray A (2003). An important regulatory role for CD4+CD8 alpha alpha T cells in the intestinal epithelial layer in the prevention of inflammatory bowel disease. *Proc Natl Acad Sci U S A* 100: 5324-5329.
- Eberle M, Ebel P, Wegner MS, Mannich J, Tafferner N, Ferreiros N, *et al.* (2014). Regulation of ceramide synthase 6 in a spontaneous experimental autoimmune encephalomyelitis model is sex dependent. *Biochem Pharmacol* 92: 326-335.
- Feillet F, Clarke L, Meli C, Lipson M, Morris AA, Harmatz P, *et al.* (2008). Pharmacokinetics of Sapropterin in Patients with Phenylketonuria. *Clin Pharmacokinet* 47: 817-825.

- Fischer MT, Sharma R, Lim JL, Haider L, Frischer JM, Drexhage J, *et al.* (2012). NADPH oxidase expression in active multiple sclerosis lesions in relation to oxidative tissue damage and mitochondrial injury. *Brain* 135: 886-899.
- Gangula PR, Challagundla KB, Ravella K, Mukhopadhyay S, Chinnathambi V, Mittal MK, *et al.* (2018). Sepiapterin alleviates impaired gastric nNOS function in spontaneous diabetic female rodents through NRF2 mRNA turnover and miRNA biogenesis pathway. *Am J Physiol Gastrointest Liver Physiol* 315: G980-g990.
- Giovannoni G, Heales SJ, Land JM, & Thompson EJ (1998). The potential role of nitric oxide in multiple sclerosis. *Mult Scler* 4:212-216.
- Gurke R, Thomas D, Schreiber Y, Schafer SMG, Fleck SC, Geisslinger G, *et al.* (2019). Determination of endocannabinoids and endocannabinoid-like substances in human K3EDTA plasma - LC-MS/MS method validation and pre-analytical characteristics. *Talanta* 204:386-394.
- Howells D, Smith I, Leonard J, & Hyland K (1986). Tetrahydrobiopterin in dihydropteridine reductase deficiency. *N Engl J Med* 314:520-521.
- Huber C, Batchelor JR, Fuchs D, Hausen A, Lang A, Niederwieser D, *et al.* (1984). Immune response-associated production of neopterin. Release from macrophages primarily under control of interferon-gamma. *J Exp Med* 160: 310-316.
- Husain N, Tokoro K, Popov JM, Naides SJ, Kwasny MJ, & Buchman AL (2013). Neopterin concentration as an index of disease activity in Crohn's disease and ulcerative colitis. *J Clin Gastroenterol* 47: 246-251.
- Jeong JH, Lee N, Tucker MA, Rodriguez-Miguel P, Looney J, Thomas J, *et al.* (2019). Tetrahydrobiopterin improves endothelial function in patients with cystic fibrosis. *Journal of applied physiology* (Bethesda, Md : 1985) 126: 60-66.
- Katusic ZS, d'Uscio LV, & Nath KA (2009). Vascular protection by tetrahydrobiopterin: progress and therapeutic prospects. *Trends Pharmacol Sci* 30: 48-54.
- Kurz J, Parnham MJ, Geisslinger G, & Schiffmann S (2018). Ceramides as Novel Disease Biomarkers. *Trends Mol Med* 23: 30205-30203.
- Li L, Chen W, Rezvan A, Jo H, & Harrison DG (2011). Tetrahydrobiopterin deficiency and nitric oxide synthase uncoupling contribute to atherosclerosis induced by disturbed flow. *Arterioscler Thromb Vasc Biol* 31: 1547-1554. doi: 1510.1161/ATVBAHA.1111.226456. Epub 222011 Apr 226421.
- Licht-Mayer S, Wimmer I, Traffehn S, Metz I, Bruck W, Bauer J, *et al.* (2015). Cell type-specific Nrf2 expression in multiple sclerosis lesions. *Acta Neuropathol* 130: 263-277.
- Linker RA, Lee DH, Ryan S, van Dam AM, Conrad R, Bista P, *et al.*(2011). Fumaric acid esters exert neuroprotective effects in neuroinflammation via activation of the Nrf2 antioxidant pathway. *Brain* 134: 678-692.
- Matyash V, Liebisch G, Kurzchalia TV, Shevchenko A, & Schwudke D (2008). Lipid extraction by methyl-tert-butyl ether for high-throughput lipidomics. *J Lipid Res* 49: 1137-1146.
- McNeill E, Crabtree MJ, Sahgal N, Patel J, Chuaiphichai S, Iqbal AJ, *et al.* (2015). Regulation of iNOS function and cellular redox state by macrophage Gch1 reveals specific requirements for tetrahydrobiopterin in NRF2 activation. *Free Radic Biol Med* 79:206-216.
- McNeill E, Stylianou E, Crabtree MJ, Harrington-Kandt R, Kolb AL, Diotallevi M, *et al.* (2018). Regulation of mycobacterial infection by macrophage Gch1 and tetrahydrobiopterin. *Nat Commun* 9: 5409.
- Mossakowski AA, Pohlan J, Bremer D, Lindquist R, Millward JM, Bock M, *et al.* (2015). Tracking CNS and systemic sources of oxidative stress during the course of chronic neuroinflammation. *Acta Neuropathol* 130: 799-814.

- Oertel S, Scholich K, Weigert A, Thomas D, Schmetzer J, Trautmann S, *et al.* (2017). Ceramide synthase 2 deficiency aggravates AOM-DSS-induced colitis in mice: role of colon barrier integrity. *Cell Mol Life Sci* 74: 3039-3055.
- Pickert G, Lim HY, Weigert A, Haussler A, Myrczek T, Waldner M, *et al.* (2013). Inhibition of GTP cyclohydrolase attenuates tumor growth by reducing angiogenesis and M2-like polarization of tumor associated macrophages. *Int J Cancer* 132: 591-604.
- Prat C, Sancho JM, Dominguez J, Xicoy B, Gimenez M, Ferra C, *et al.* (2008). Evaluation of procalcitonin, neopterin, C-reactive protein, IL-6 and IL-8 as a diagnostic marker of infection in patients with febrile neutropenia. *Leuk Lymphoma* 49: 1752-1761.
- Rao RP, Yuan C, Allegood JC, Rawat SS, Edwards MB, Wang X, *et al.* (2007). Ceramide transfer protein function is essential for normal oxidative stress response and lifespan. *Proc Natl Acad Sci U S A* 104: 11364-11369.
- Rodriguez-Miguel P, Gregg J, Seigler N, Bass L, Thomas J, Pollock JS, *et al.* (2018). Acute Tetrahydrobiopterin Improves Endothelial Function in Patients With COPD. *Chest* 154: 597-606.
- Schiffmann S, Ferreiros N, Birod K, Eberle M, Schreiber Y, Pfeilschifter W, *et al.* (2012). Ceramide synthase 6 plays a critical role in the development of experimental autoimmune encephalomyelitis. *J Immunol* 188: 5723-5733.
- Schmitz K, Brunkhorst R, de Bruin N, Mayer CA, Haussler A, Ferreiros N, *et al.* (2017). Dysregulation of lysophosphatidic acids in multiple sclerosis and autoimmune encephalomyelitis. *Acta Neuropathol Commun* 5: 42.
- Schmitz K, de Bruin N, Bishay P, Mannich J, Haussler A, Altmann C, *et al.* (2014). R-flurbiprofen attenuates experimental autoimmune encephalomyelitis in mice. *EMBO Mol Med* 6: 1398-1422.
- Schmitz K, Wilken-Schmitz A, Vasic V, Brunkhorst R, Schmidt M, & Tegeder I (2019). Progranulin deficiency confers resistance to autoimmune encephalomyelitis in mice. *Cell Mol Immunol*.
- Schoedon G, Troppmair J, Adolf G, Huber C, & Niederwieser A (1986). Interferon-gamma enhances biosynthesis of pterins in peripheral blood mononuclear cells by induction of GTP-cyclohydrolase I activity. *J Interferon Res* 6: 697-703.
- Silva LC, de Almeida RF, Castro BM, Fedorov A, & Prieto M (2007). Ceramide-domain formation and collapse in lipid rafts: membrane reorganization by an apoptotic lipid. *Biophys J* 92: 502-516.
- Sucher R, Schroecksnadel K, Weiss G, Margreiter R, Fuchs D, & Brandacher G (2010). Neopterin, a prognostic marker in human malignancies. *Cancer Lett* 287: 13-22.
- Tegeder I, Adolph J, Schmidt H, Woolf CJ, Geisslinger G, & Lotsch J (2008). Reduced hyperalgesia in homozygous carriers of a GTP cyclohydrolase 1 haplotype. *Eur J Pain* 12: 1069-1077.
- Thiel VE, & Audus KL (2001). Nitric oxide and blood-brain barrier integrity. *Antioxid Redox Signal* 3: 273-278.
- Watschinger K, Keller MA, Golderer G, Hermann M, Maglione M, Sarg B, *et al.* (2010). Identification of the gene encoding alkylglycerol monooxygenase defines a third class of tetrahydrobiopterin-dependent enzymes. *Proc Natl Acad Sci U S A* 107: 13672-13677.
- Watschinger K, Keller MA, McNeill E, Alam MT, Lai S, Sailer S, *et al.* (2015). Tetrahydrobiopterin and alkylglycerol monooxygenase substantially alter the murine macrophage lipidome. *Proc Natl Acad Sci U S A* 112: 2431-2436.
- Werner ER, Blau N, & Thony B (2011). Tetrahydrobiopterin: biochemistry and pathophysiology. *Biochem J* 438: 397-414.

Williams A, Eldridge R, Levine R, Lovenberg W, & Paulson G (1979). Low CSF hydroxylase cofactor (tetrahydrobiopterin) levels in inherited dystonia. *Lancet* 2: 410-411.

Wu M, & Tsirka SE (2009). Endothelial NOS-deficient mice reveal dual roles for nitric oxide during experimental autoimmune encephalomyelitis. *Glia* 57: 1204-1215.

Zhao J, Shi P, Sun Y, Sun J, Dong JN, Wang HG, *et al.* (2015). DHA protects against experimental colitis in IL-10-deficient mice associated with the modulation of intestinal epithelial barrier function. *Br J Nutr* 114: 181-188.

Zschiebsch K, Fischer C, Pickert G, Haussler A, Radeke H, Grosch S, *et al.* (2016). Tetrahydrobiopterin Attenuates DSS-evoked Colitis in Mice by Rebalancing Redox and Lipid Signalling. *J Crohns Colitis* 10: 965-978.

Acknowledgement and funding

The study was supported by the Deutsche Forschungsgemeinschaft (SFB815, A12 to IT and CRC1039 A03 to IT and CRC1039 Z01 to GG) and the Fraunhofer Cluster of Excellence for immune mediated diseases (CIMD). The funding institution had no role in the conceptualization, design, data collection, analysis, decision to publish, or preparation of the manuscript.

Competing interests

The authors declare that they have no competing financial interests or other competing interests that might be perceived to influence the results and/or discussion reported in this paper.

Data availability statement

Microarray datasets have been deposited previously and are available as GEO dataset with the accession number GSE60847.

Author contributions

KS did the EAE studies, FACS analyses, histology and analyzed data. CF analyzed AGMO-LacZ mice. ST, YS, LH and DT analyzed lipid concentrations. IT initiated the study, devised and organized the experiments and analyzed data, created the figures and wrote the manuscript. RB and SW recruited patients and controls. ERW and KW generated AGMO-LacZ mice. DT and GG organized the analytical lipid lab. All authors contributed to manuscript drafting, reviewed the manuscript and approved the final version of the manuscript.

Figure legends

Figure 1

Biopterin and Neopterin in human multiple sclerosis

A: Biopterin and neopterin concentrations in plasma or serum in two cohorts of patients with multiple sclerosis (MS-1 n = 102; MS-2 n = 14 with repeated samples over time) as compared to biopterin/neopterin

in four cohorts of healthy control subjects of different ages. The gender distribution was 2:1 women/men in MS patients as well as in healthy cohorts. The time courses are shown in C. The box shows the interquartile range, the line is the median, whiskers show minimum to maximum. Each scatter represents one subject except in the right plot, where each scatter is one sample. Data were compared with two-way ANOVA for "pterin X group" and subsequent posthoc t-test for group using an adjustment of alpha according to and Šidák. *P < 0.05, **P < 0.01, ***P < 0.001.

B: Serum biopterin concentrations of MS cohort-1 categorized according to ICD10 criteria as compared to healthy controls. Each scatter is a patient or healthy control. The box shows the interquartile range, the line is the median, whiskers show minimum to maximum. Data were compared with two-way ANOVA for "pterin X group" and subsequent posthoc t-test for group using an adjustment of alpha according to and Šidák. *P < 0.05, **P < 0.01, ***P < 0.001.

C: Time courses of serum biopterin and neopterin concentrations in 14 MS patients with complicated MS course. The X-axis shows the days since diagnosis, which was day zero. The dashed lines show the mean biopterin (B) or neopterin (N) concentration in healthy controls. Arrows point to relapses (R) without or with steroid medication (R/S). Patients received fingolimod (FG), natalizumab (Ntx) or rituximab (Rtx) as indicated. Biopterin was persistently low, not obviously in association with relapse or medication.

D: Plasma concentrations of biopterin in a human whole blood assay upon stimulation with lipopolysaccharide, LPS versus vehicle (mean, SD). Biopterin levels drop over time in LPS stimulated samples. Each scatter is one healthy donor (n = 13), whose blood samples were split in two, one for LPS the other as control. The middle panel shows the paired analyses of the subject's LPS and vehicle samples at different time points. Paired data were compared by paired t-tests and time courses per 2-way ANOVA for "time X treatment".

Figure 2

Effects of sapropterin medication on the disease severity in EAE mice

A: Time courses of the clinical EAE scores (median \pm siqr), body weights (mean \pm SD), score frequency distribution and AUCs of score of SJL/J mice in PLP-induced relapsing-remitting EAE. Mice were treated orally with vehicle (2% DMSO), sapropterin (2 mg/d) or DAHP (4 mg/d) in the drinking water starting at the day of immunization. The score courses were analyzed using Friedmann statistics, the score frequency distribution using the ChiSquare test and the AUCs of the scores were compared with the Kruskal Wallis test (n = 6-8 per group).

B: Time courses of the clinical EAE scores, body weights, score frequency distribution and AUCs of EAE scores in C57Bl6/J mice in MOG-induced primary progressive EAE. Mice were treated orally with vehicle or sapropterin soaked cornflakes once daily (dosages as in A). The score courses were analyzed using Wilcoxon P statistics, the score frequency distribution using the ChiSquare test and the AUCs of the scores were compared with the Mann Whitney U test (n = 10 per group).

The box plots in A and B show the interquartile range, the line is the median, whiskers show minimum to maximum, each scatter is a mouse.

Figure 3:

FACS analyses of immune cells in the spinal cord of EAE mice

A: FACS analysis of lumbar spinal cord cells from vehicle or sapropterin (BH4) treated C57Bl6/J-EAE mice. The tissue was dissected 19 days after immunization and 300000 cells were counted of each seven mice. The dot plot shows exemplary cell clouds gated according to forward scatter (FSC) versus sideward scatter (SSC). The gates show lymphocytes and monocytes according to size and granularity. The bar chart shows the frequency of lymphocytes as percentage of viable cells (compared per unpaired, 2-sided t-test; *P < 0.05). CD4 and CD8 positive T-cells subpopulations are shown in the right panel histograms.

B: FACS analysis of lumbar spinal cord cells as in A. Immune cells were further analyzed for F4/80 and CD36 (exemplary dot plot, middle). The box plot shows the frequency of myeloid subpopulations (as percentage of all immune cells). The box is the interquartile range, whiskers show minimum to maximum, the line is the median. Each scatter is one mouse.

Figure 4:

Immunofluorescence analyses of immune cell infiltration of the spinal cord in EAE mice

C57Bl6/J mice were immunized with MOG and treated with vehicle or sapropterin (BH4) starting at the day of immunization. The tissue was prepared 19 days after immunization. Myeloid cells were stained with anti CD11b, Iba1 and F4/80. T-cells were identified via anti-CD3. NeuN was used as neuronal counterstain, and DAPI to label nuclei. For the overviews, tiled images were captured and stitched. Scale bars are 500 μm , and 20 μm (zoom in).

Figure 5:

Targeted and untargeted lipidomic analyses of bioactive and metabolic lipids in plasma in EAE mice

A: Scatter plots of regulated fatty acid associated genes (microarray) in the spinal cord of C57BL6 EAE mice versus control mice (CFA without MOG) 16 days after immunization (GSE GSE60847). Volcano plot overviews in Suppl. Fig. 1.

B: Volcano plot show the \log_2 difference (= fold difference; X-axis) of metabolic plasma lipids between sapropterin and vehicle treated EAE mice versus the $-\log_{10}$ of the P-value of the t-test (Y-axis). Lipids that were reduced in sapropterin-treated mice appear on the left side of the Y-axis, increased lipids on the right side.

C: The box/scatter plot shows the \log_2 transformed levels of fatty acids. The data represent the ratios of the mass spectrometry peak areas normalized by the peak areas of the respective standard. The box represents the IQR, whiskers show minimum to maximum, the line is the median. Each scatter is a mouse (n = 10 per group). Data were compared with two-way ANOVA for "fatty acid X treatment" and subsequent posthoc analysis for treatment using an adjustment of alpha according to Šidák.

D: Canonical discriminant score plots of the first discriminant factors CanDis1 and CanDisc2 for plasma lipids using 28 lipid species of five classes as input. The plasma concentrations were obtained from SJL/J mice immunized with PLP and treated orally with vehicle (2% DMSO), sapropterin (2 mg/d) or DHAP (4 mg/d) via the drinking water starting at the day of immunization (n=7 per group). The final blood sample for lipid analyses was obtained 22 days after immunization. Lipids encompassed ceramides, hexosylceramides, sphingolipids, endocannabinoids and lysophosphatidic acids (individually presented in Suppl. Fig. 3). The dots show individual mice. The ellipses show the 95% confidence.

E: Box/scatter plots of normalized ceramides and endocannabinoids in vehicle, sapropterin (BH4) or DAHP treated SJL/J-EAE mice as in A. Lipids were normalized as percentages of the 90%-quantile (raw concentrations shown in Suppl. Fig. 3). The box represents the interquartile range, whiskers show minimum to maximum, the line is the median. Each scatter is a mouse. Data were compared with two-way ANOVA for "lipid X treatment" and subsequent posthoc analysis for treatment using an adjustment of alpha according to Šidák (n = 6-8 per group, * P < 0.05, ** P < 0.001).

F: Polar plots show the mean normalized levels (percentages of the 90% quantile) of multiple lipid species analyzed via targeted LC-MS/MS analyses in plasma of SJL/J-EAE mice treated as in A. Most ceramides and some lysophosphatidic acids (LPAs) were increased in sapropterin-treated mice.

Figure 2

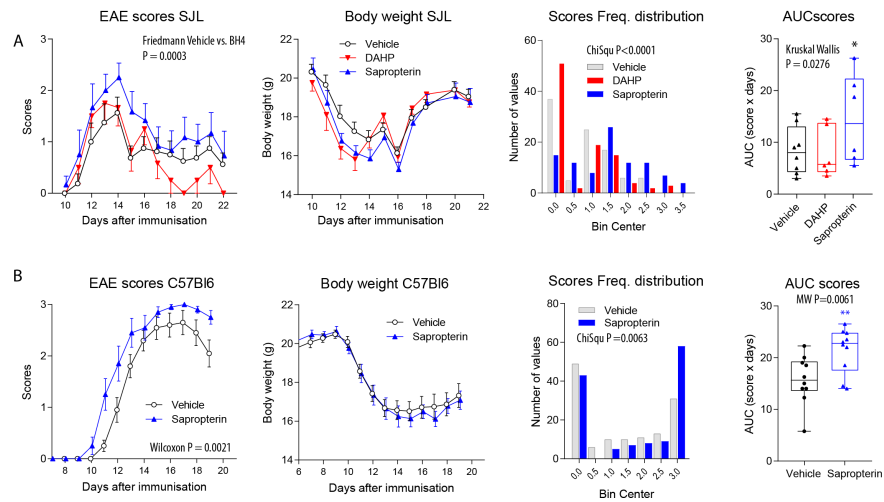


Figure 3

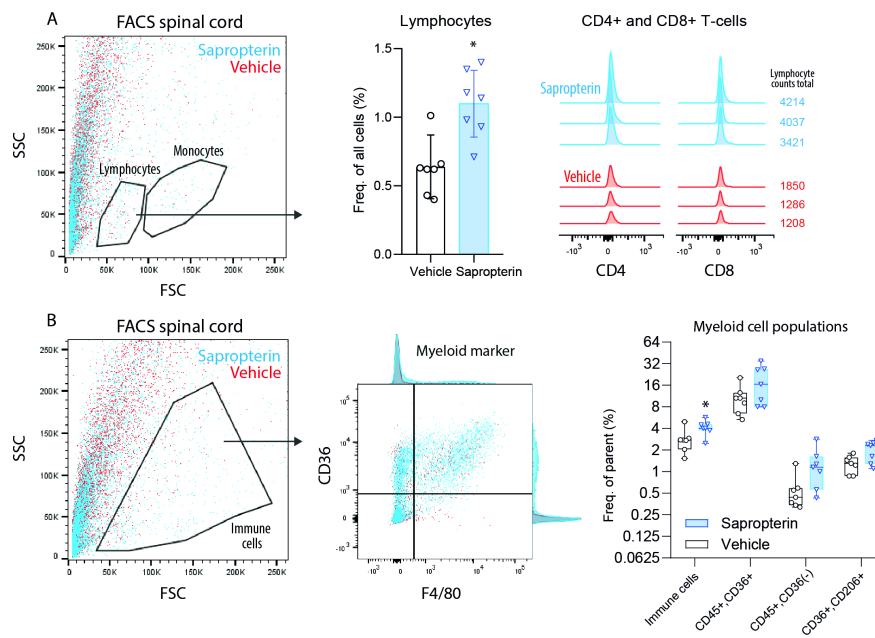


Figure 5

